JACS
JOURNAL OF THE AMERICAN CHEMICAL SOCIETY

Article

pubs.acs.org/JACS

Enabling Förster Resonance Energy Transfer from Large Nanocrystals through Energy Migration

Renren Deng,[†,∥] Juan Wang,[†,∥] Runfeng Chen,[‡] Wei Huang,[*,‡,§] and Xiaogang Liu[*,†,⊥]

[†]Department of Chemistry, National University of Singapore, Singapore 117543

[‡]Key Laboratory for Organic Electronics and Information Displays & Institute of Advanced Materials, Jiangsu National Synergetic Innovation Center for Advanced Materials, Nanjing University of Posts and Telecommunications, Nanjing 210023, China

[§]Key Laboratory of Flexible Electronics and Institute of Advanced Materials, Jiangsu National Synergetic Innovation Center for Advanced Materials, Nanjing Tech University, Nanjing 211816, China

[⊥]Institute of Materials Research and Engineering, Singapore 138634

Supporting Information

ABSTRACT: The stringent distance dependence of Förster resonance energy transfer (FRET) has limited the ability of an energy donor to donate excitation energy to an acceptor over a Förster critical distance (R_0) of 2−6 nm. This poses a fundamental size constraint (<8 nm or ~$4R_0$) for experimentation requiring particle-based energy donors. Here, we describe a spatial distribution function model and theoretically validate that the particle size constraint can be mitigated through coupling FRET with a resonant energy migration process. By combining excitation energy migration and surface trapping, we demonstrate experimentally an over 600-fold enhancement over acceptor emission for large nanocrystals (30 nm or ~$15R_0$) with surface-anchored molecular acceptors. Our work shows that the migration-coupled approach can dramatically improve sensitivity in FRET-limited measurement, with potential applications ranging from facile photochemical synthesis to biological sensing and imaging at the single-molecule level.

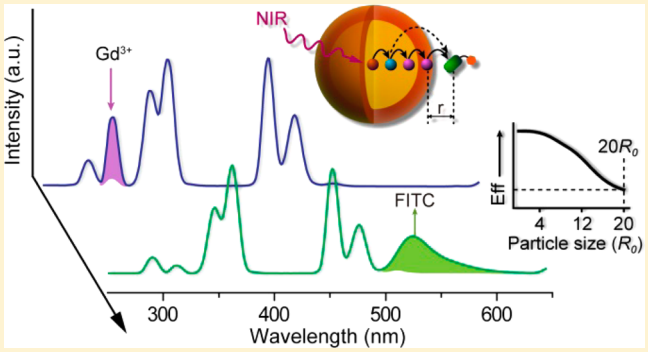

INTRODUCTION

The fundamental understanding of Förster resonance energy transfer (FRET) between two adjacent molecules through nonradiative dipole−dipole coupling is essential for probing nanoscale physiological processes and for a number of applications, including remote sensing, cellular imaging, single-molecule spectroscopy, and optoelectronics.[1] Since the groundbreaking experimental study of colloidal semiconductor nanocrystals as FRET donors by Medintz et al.,[1d] the field of FRET investigations has broadened to include large classes of nanomaterials. These include quantum dots, carbon-based nanostructures, plasmonic metal nanoparticles, and lanthanide-doped nanophosphors.[2]

The FRET process involving a given set of molecular and nanoparticle components is often difficult to control and is critically dependent upon the donor−acceptor distance. For molecule−nanoparticle hybrid systems, the FRET efficiency is expected to diminish drastically. This constraint arises because the dimensions of the particle components, serving either as FRET donors or acceptors, are generally much greater than the Förster critical distance, at which the energy transfer rate is equal to the internal decay rate of the donor.[1c,3] Although various efforts have been explored, achieving efficient long-range FRET in large-sized donor−acceptor systems remains a major challenge.

Herein, we report a design principle that can be used to maximize energy propagation between a nanoparticle donor and an organic dye acceptor, based on spatial energy migration through gadolinium (Gd^{3+}) sublattices. With this design, highly efficient FRET is possible for particle-based donor systems with sizes significantly larger than the Förster critical distance. For instance, our experimental results show over a 600-fold enhancement in dye acceptor emission using $NaGdF_4$-based particle donors (~30 nm) compared with commonly used $NaYF_4$-based particles.

THEORETICAL MODELS

We set out to demonstrate the utility of migration coupling by investigating the theoretical limits of FRET in typical nanoparticle-based systems. Let us consider each dopant ion in a nanoparticle as an individual energy donor. Thus, the energy transfer processes from a lanthanide-doped nanoparticle to many surface-conjugated energy acceptors can be principally treated as the sum of the energy transfer from each dopant ion

Received: September 5, 2016
Published: November 16, 2016

DOI: 10.1021/jacs.6b09349
J. Am. Chem. Soc. 2016, 138, 15972−15979

to all acceptors within the single particle. The overall efficiency of the energy transfer can be quantitatively calculated by averaging all possible distributions of acceptor−donor pairs. Based on this consideration, the energy transfer from the nanoparticle to many energy acceptors can be described by the following models.

For simplicity, we assume that the nanoparticle is spherical with a radius of R, and the distribution of acceptors on a large number of nanoparticles follows the Poisson law.[4] Considering the excitation of an individual nanoparticle by a beam of light, we describe the time evolution of the excited state of the donor D^* as

$$dD^*/dt = \delta(t) - k_D D^* - k_{DA} D^* \tag{1}$$

and

$$k_D = k_0 = 1/\tau_D \tag{2}$$

where $\delta(t)$ is a time-dependent function related to the profile of the excitation light, k_D and τ_D are the respective radiative rate and luminescence lifetime of the donor in the absence of the acceptor, and k_{DA} is the rate constant describing the total energy transfer contributions from all donor−acceptor pairs.

Assuming that the nanoparticle contains n possible donor−acceptor pairs with distances of r_1, r_2, r_3,...r_n and $k(r_i)$ represents the energy transfer rate between ith donor−acceptor pair, k_{DA} can be written as

$$k_{DA} = \sum_{i=1}^{n} k_i = \sum_{i=1}^{n} k(r_i) \tag{3}$$

Suppose that the excitation is an infinitely short pulse by which $\delta(t) > 0$ when $t = 0$ and $\delta(t) = 0$ when $t > 0$, the solution of eq 1 can be expressed by the following equation

$$\rho D^*(t) = \exp(-k_D t - k_{DA} t) \tag{4}$$

or

$$I(t) = I(0)\exp(-k_D t - k_{DA} t) \tag{5}$$

where $\rho D^*(t)$ is the probability of finding the donor at the excited state at a given time t, and $I(t)$ is the emission intensity of the donor recorded at time t.

Direct FRET. In this case, only donor−acceptor interactions are taken into account. The excited energy donors directly transfer their energy to acceptors without any donor−donor interaction.[5] Combining eq 2, eq 3, and eq 4, $\rho D^*(t)$ can be obtained as

$$\rho_n D^*(t) = \exp(-k_0 t - \sum_{i=1}^{n} k_i t) = \prod_{i=0}^{n} \exp(-k_i t) \tag{6}$$

If the spatial distribution of the energy donors and acceptors follows a function $P(r)$,[5a] we can define the $P(r)dr$ as the probability of finding an acceptor in the distance interval of $[r, r + dr]$ from the donor. $\rho D^*(t)$ can be further written as

$$\rho_n D^*(t) = \int\int \ldots \int \prod_{i=0}^{n} \{P(r_i)\exp[-k(r_i)t]\} dr_0 dr_1 \ldots dr_n \tag{7}$$

which can be rewritten as

$$\rho_n D^*(t) = Q(r)^n \exp(-k_0 t) = Q(r)^n \exp(-t/\tau_D) \tag{8}$$

in which

$$Q(r) = \int P(r)\exp[-k(r)t] dr \tag{9}$$

Considering the Poisson distribution of energy acceptors and the average number of acceptor molecules μ attached to each nanoparticle, we have

$$\rho D^* = \sum_{n=0}^{\infty} \frac{\rho_n D^*(t) \mu^n \exp(-\mu)}{n!} = \exp(-t/\tau_D)\exp(-\mu) \sum_{n=0}^{\infty} \frac{(Q\mu)^n}{n!} \tag{10}$$

By introducing a suitable distribution function of $P(r)$ and distance-dependent energy transfer rate constant $k(r)$, eq 11 can be generalized to describe any given direct FRET processes.

$$\rho D^* = \exp(-t/\tau_D)\exp\{-\mu[1 - Q(r)]\} \tag{11}$$

We can then obtain the simulated decay curve of donor emission from eq 12 as

$$I(t) = I(0)\exp(-t/\tau_D)\exp\{-\mu[1 - Q(r)]\} \tag{12}$$

or the expression of the direct FRET efficiency Eff by

$$\text{Eff} = 1 - \phi_{DA}/\phi_D = 1 - \frac{1}{\tau_D}\int_0^{\infty} \exp\{-t/\tau_D - \mu[1 - Q(r)]\} dt \tag{13}$$

Migration-Coupled FRET. In the direct FRET model, the energy transfer rate k for any given donor−acceptor pairs only depends on their separation distance r. This likely leads to spatial inhomogeneity in excitation energy distribution during the FRET process because donors can transfer their excitation energy to the acceptors placed in close proximity at significantly faster rates.[6] Notably, the inhomogeneous distribution of the excitation energy can be minimized by spreading out the excited energy over many energy donors within the nanoparticle through interparticle energy transfer. As such, we need to consider additional donor−donor interactions in deriving k_{DA}.

Despite the extreme complexity in the energy migration process and the variable nature of k_{DA} over time, we can approximately derive an average k_{DA} in the form of $\bar{k}_{DA}$ according to the energy migration and trapping model developed by Burshtein and Blasse.[7] Considering the spatial distribution function $P(r)$ for both donors and acceptors, the energy transfer is obtained by

$$\bar{k}_{DA} = \frac{1}{\tau_1^2}\int_0^{\infty} \mu[1 - Q(r)]\exp(-t/\tau_1) dt = \int \mu P(r) \frac{k(r)}{1 + k(r)\tau_1} dr \tag{14}$$

where $k(r)$ is as the same constant as that in eq 9 and represents the rate of energy transfer from the donor to the acceptor, τ_1 is the average hopping time of energy migration, and $1/\tau_1$ represents the probability of energy transfer between any given donors (Supporting Information section 5). Thereafter, we can get the expression for the migration-coupled FRET efficiency as

$$\text{Eff} = 1 - \frac{1}{\tau_D}\int_0^{\infty} \exp(-t/\tau_D - \bar{k}_{DA} t) dt \tag{15}$$

DOI: 10.1021/jacs.6b09349
J. Am. Chem. Soc. 2016, 138, 15972−15979

RESULTS AND DISCUSSION

The models above are based on the calculation of the summation of energy transfer from every possible parts of the nanoparticle to any given acceptors. To statistically quantify the separating distance between the dye acceptor and different parts of the particle donor, we introduced a spatial distribution function $P(r)$.[5a] For instance, $P(r) = (3r^2/4R^3)(2R - r)$ for a molecular acceptor attached on a particle with a diameter of R (Supporting Information). For direct FRET process, the distance-dependent rate constant $k(r)$ is proportion to R_0^6/r^6, where R_0 is the Förster critical distance (typically in the range of 2−6 nm).[1b] According to eq 13, the energy transfers Eff approaches nearly zero for a particle size of ~$4R_0$ (8−24 nm), which apparently places a strong size constraint on this direct FRET mechanism (Figure 1a).

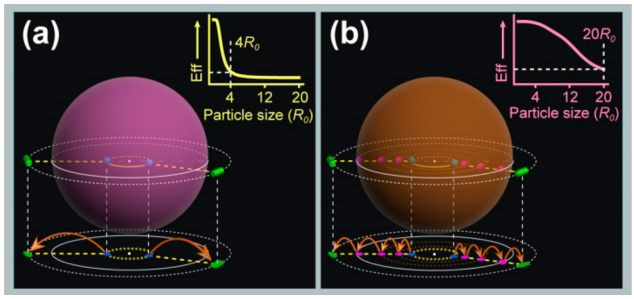

Figure 1. (a) Direct FRET modeling showing that the luminescent centers (represented as blue spheres) buried inside the nanoparticle directly transfer their excitation energy to proximal molecular acceptors (represented as green cylindrical rods) through dipole−dipole interaction. (b) Migration-coupled FRET model highlighting an enabled long-distance energy transfer between the pair by the process of energy migration among luminescent centers (represented as purple spheres). Inset: FRET efficiency (Eff) obtained as a function of particle size in two different models. Note that the efficiency was calculated on the basis of energy transfer from a single nanoparticle to a single molecular acceptor. R_0 is the Förster critical radius and in the range of 2−6 nm.

We reasoned that the size constraint on the efficiency of FRET may be dramatically minimized through intraparticle energy migration by which the excitation energy can be confined to the particle surface and ultimately directed to the molecular acceptor with a high yield. In previous studies, the mode of energy migration was basically treated as a stochastic process of hopping.[7] To quantitatively describe the contribution of a migration-coupled FRET process, we combined the spatial distribution function $P(r)$ with the models developed by Burshtein and Blasse. The resulting excitation transfer function can then be expressed by eq 15. This newly developed function reveals that the migration of optical energy among the luminescent centers, interspersedly stationed in the nanoparticle, indeed facilitates FRET relaxation (Supporting Information). For instance, even for a particle of ~$20R_0$ (40−120 nm), an Eff value of almost 10% is still achievable by taking advantages of the migration coupling (Figure 1b).

Encouraged by the theoretical prediction, we next experimentally validate the migration coupling effect on FRET efficiency using a series of Gd^{3+}-based nanocrystals as a model system. We choose the Gd^{3+}-based host material because it boosts sublattice-mediated energy migration over long distances.[8] It is also important to note that Gd^{3+} features a large energy gap (~4.0 eV) between its ground state ($^8S_{7/2}$) and lowest excited state ($^6P_{7/2}$), so that the conditions for excitation energy deactivation through nonradiative pathways is considerably less favorable.[9]

In a typical study of migration coupling, we first prepared $NaGdF_4$:Yb/Tm nanoparticles coated with a thin layer of $NaGdF_4$ (Supporting Information). In this material, Yb/Tm was codoped to realize visible and ultraviolet upconversion emission from Tm^{3+} under near-infrared excitation. Gd^{3+} sublattice is capable of extracting upconverted photon energy from the Yb^{3+}/Tm^{3+} codoped system and subsequently transporting the energy from the core to the shell layer of the nanoparticle.[8b,c] This process allows the excitation energy to be migrated to the particle's surface, thereby promoting the transfer of energy from the particle to surface-tethered molecular acceptors. It should be mentioned that the core−shell design not only enables the energy migration within Gd^{3+}-based shell layer but also helps protect active dopants (Yb^{3+} and Tm^{3+}) in the core from surface quenching-induced energy loss. Transmission electron microscopy (TEM) showed a spherical shape of the particles having an average diameter of 30 nm and a shell thickness of ~2.5 nm (Figure S1). By adopting the same method, we also prepared $NaYF_4$:Yb/Tm@$NaYF_4$ core−shell nanoparticles (~30 nm) and $NaYF_4$:Yb/Tm nanoparticles (~25 nm) as controls (Figure S2). Since Y^{3+} does not have any energy level that matches with the emitting states of Tm^{3+}, we would expect no migration coupling in these control particles. These newly synthesized nanoparticles were then coated with a thin silica layer and further conjugated with fluorescein isothiocyanate (FITC), a dye molecule widely used as the energy acceptor for FRET investigations because of strong fluorescence from its singlet state (lifetime 4.1 ns) (Experimental Section and Figures S3−S7). The size of the dye molecule (~1 nm) is much smaller than that of the nanoparticle, and thus the particle does not possess the ability to deliver most of its excitation energy to the dye acceptor by the process of direct FRET (Figure 2a).

We subsequently measured the luminescence profile of $NaGdF_4$:Yb/Tm@$NaGdF_4$ nanoparticles with and without the attachment of FITC molecules. In the absence of the dye acceptor, these nanoparticles showed four emission bands centered around 290, 310, 350, and 460 nm when illuminated at 980 nm (Figure 2b). The emission signal at 310 nm results from the $^6P_{7/2} \rightarrow {}^8S_{7/2}$ transition of Gd^{3+}, while the rest of the emission bands is characteristic of direct emission from Tm^{3+}.[10] The emission spectrum of the nanoparticle overlaps with the absorption spectrum of the dye acceptor over a broad wavelength range, which makes possible the transfer of excitation energy between the pair (Figure 2b). As such, the Förster critical radius R_0 of the dye−particle system was estimated to be 2 nm, which is 15 times smaller than the diameter of the core−shell nanoparticle under investigation.[11] The photoluminescence spectrum, nevertheless, suggests that an efficient FRET process has occurred from the nanoparticle to the FITC molecule, as evidenced by the strong depression of Gd^{3+} emission at 310 nm and the concurrent increase in FITC fluorescence at 520 nm (Figure 3 and Figure S9). In stark contrast, under identical conditions, the FITC emission intensity was found to be 25 and 635 times lower when $NaYF_4$:Yb/Tm@$NaYF_4$ core−shell nanoparticles and $NaYF_4$:Yb/Tm core-only nanoparticles were used as the energy donor, respectively (Figures 3 and 4). This is rather surprising, considering that the overall emission intensity of the $NaYF_4$ core−shell nanoparticles is 2 times stronger than that of the

DOI: 10.1021/jacs.6b09349
J. Am. Chem. Soc. 2016, 138, 15972−15979

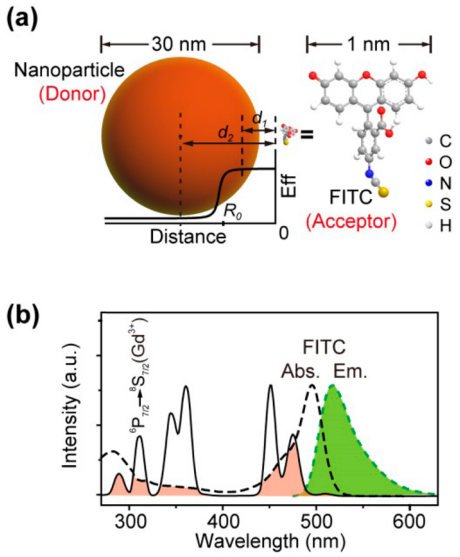

Figure 2. (a) Schematic presentation showing the dimensions of a nanoparticle donor (~30 nm) and a FITC dye acceptor (~1 nm). It is also shown that the FRET efficiency (Eff) critically depends on the distance separating the dye molecule and the luminescent center ($d_2 > R_0 > d_1$). (b) Absorption (Abs.) and emission (Em.) spectra of the FITC molecules and $NaGdF_4$:Yb/Tm@$NaGdF_4$ upconversion nanoparticles. The spectral overlapping between the emission of the nanoparticles and the absorption of the FITC molecules is highlighted in orange.

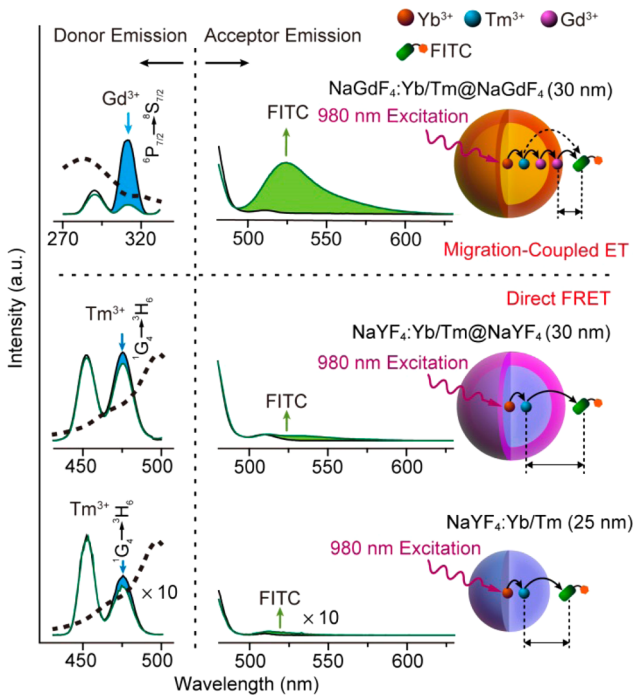

Figure 3. Luminescence spectra of particle (left panels) and sensitized dye (right panels) emissions recorded before (black line) and after (dark green line) FITC–particle conjugation. The black dashed lines in the left panels are the corresponding absorption spectra of FITC. The changes in the emission intensity of the nanoparticles and sensitized FITC molecules are highlighted in blue and green, respectively. The inseted drawings show the proposed energy transfer processes dominated in different FITC–nanoparticle systems under investigation.

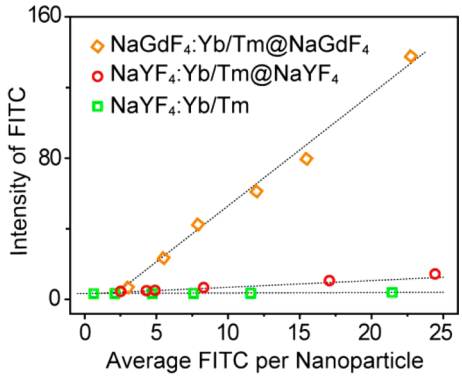

Figure 4. Integrated emission intensities of FITC plotted against its surface density for different types of nanoparticles. The intensity profiles were integrated over the spectral range of 500–600 nm following a 980 nm illumination.

$NaGdF_4$ counterparts (Figure S5). In addition, although the core-only particles may exhibit FRET efficiency higher than that of their core–shell counterparts because of their smaller size, the intensity of the FITC emission caused by FRET from the core-only particles turns out to be much lower due to the weaker overall emission intensity (Figure S5).

The dynamic optical characterizations of the samples provide more definitive evidence for the critical role of migration coupling in enhancing energy transfer from lanthanide-doped nanoparticles. For instance, time-resolved photoluminescence spectroscopic investigations of FITC-conjugated $NaGdF_4$:Yb/Tm@$NaGdF_4$ nanoparticles reveals a significant shortening in the lifetime of Gd^{3+} emission at 310 nm, invariably accompanied by a rise in the lifetime of FITC emission centered around 520 nm (Figure 5a,b). On the other hand, the lifetime of the emission arising from Tm^{3+} activator remains virtually unaltered before and after the attachment of FITC molecules to the nanoparticles (Figure 5a–c and Figure S10). Taken together, these results indicate that the energy transfer and migration pathway is likely to take place through $Tm^{3+} \rightarrow Gd^{3+} \rightarrow$ FITC rather than by the direct FRET process through $Tm^{3+} \rightarrow$ FITC. The Eff of the energy transfer can be calculated as $1 - \tau_{DA}/\tau_D$, where τ_{DA} is the luminescence lifetime of the particle donor in the presence of energy acceptors. A quantitative measurement of the energy transfer efficiency reveals that an average of 22 FITC molecules per particle can lead to 91 ± 4% efficiency through migration-coupled energy transfer, whereas the measured efficiency is less than 5% for a direct energy transfer from Tm^{3+} to FITC involving a similar number of FITC molecules per particle. It is important to note that the experimental results of the energy transfer efficiency are in good agreement with our model simulations fitted by eqs 2 and 3 (Figure 5d).

Of special significance is the fast migration of excitation energy through the Gd sublattice during the natural lifetime of the excited Gd^{3+}. In the case of a $NaGdF_4$ crystal, our calculation shows that the energy is able to move ~1.3×10^5 steps on average if there are no energy acceptors or defect sites present in the lattice (Supporting Information section 5). This movement amounts to a large energy propagation distance of ~140 nm (Supporting Information section 5). In the presence of surface-bound energy acceptors, random-walk Monte Carlo simulations of a $NaGdF_4$:Yb/Tm@$NaGdF_4$ nanoparticle reveal that more than 95% of the excitation energy, dominated by the Gd sublattice in the particle core, can be directed to the particle

DOI: 10.1021/jacs.6b09349
J. Am. Chem. Soc. 2016, 138, 15972–15979

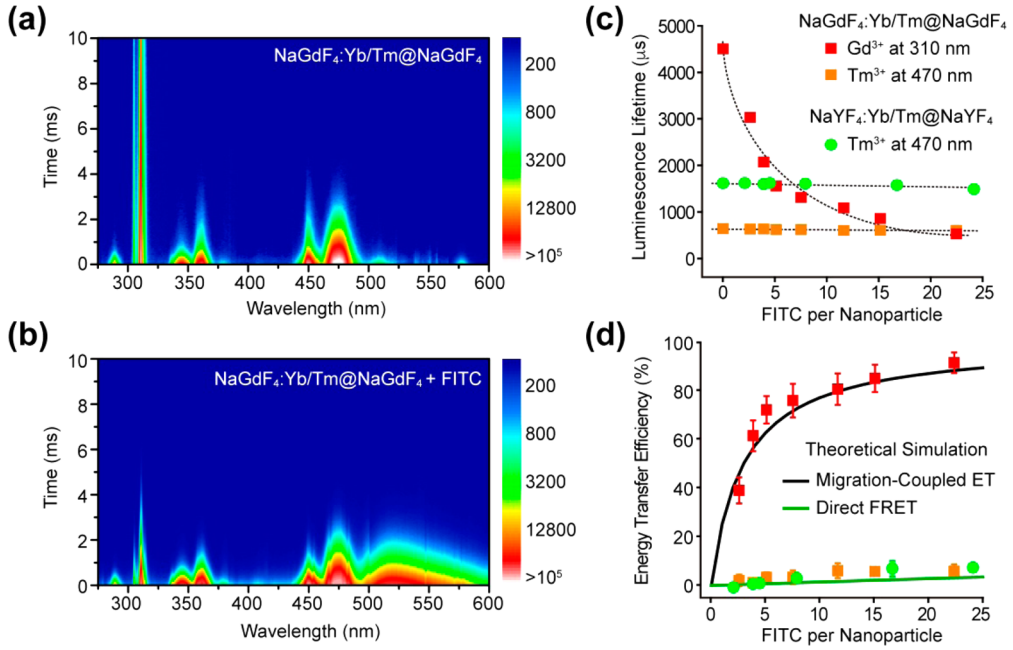

Figure 5. (a) Time-resolved upconversion luminescence mapping of 30 nm $NaGdF_4$:Yb/Tm@$NaGdF_4$ nanoparticles in the absence of FITC. Note that the long-lasting emission ($\tau_D \sim 4.5$ ms) at 310 nm is ascribed to the radiative energy transition of Gd^{3+} ($^6P_{7/2} \rightarrow {}^8S_{7/2}$). (b) Time-resolved upconversion luminescence mapping of 30 nm $NaGdF_4$:Yb/Tm@$NaGdF_4$ nanoparticles coupled with FITC. It is apparent that the lifetime of Gd^{3+} emission at 310 nm is sharply depressed, accompanied by the emergence of a broad-band emission of FITC at 500−600 nm. (c) Luminescence lifetime measurements plotted against the number of FITC molecules per nanoparticle. (d) Corresponding energy transfer efficiency curves plotted as a function of FITC molecules per nanoparticle. The efficiencies simulated by modeling migration-coupled energy transfer or direct FRET are presented in black and green lines, respectively. The experimental results are obtained from the samples shown in (c).

surface (Figure 6a). This contrasts sharply with energy patterns observed for $NaYF_4$-based analogues, wherein the excitation energy is spatially confined to the particle core and hence largely inaccessible to the surface-anchored acceptors (Figure 6b).

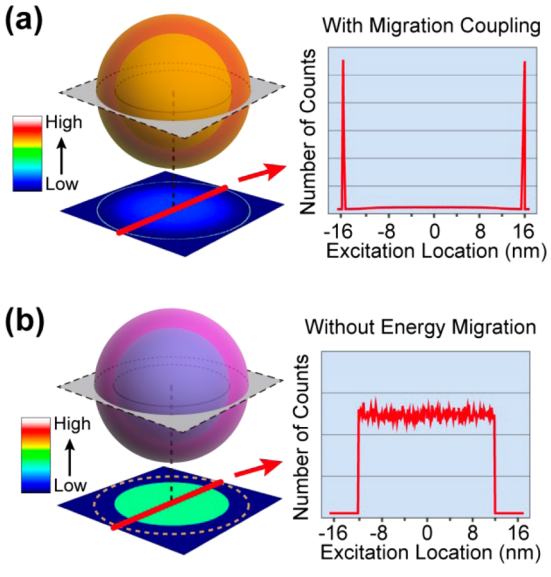

Figure 6. (a) Monte Carlo simulation of energy migration in a core−shell upconversion nanoparticle (30 nm) showing the feasibility of directing excited energy through long-range migration coupling to any given energy acceptors tethered to the particle's surface. The left and right panels show a cross-sectional view of the excitation energy mapping and its corresponding line scan, respectively, in the presence of the energy acceptors. (b) Monte Carlo simulation results of the excitation energy distribution obtained without involvement of energy migration in the core−shell nanoparticle.

We next asked whether it would be possible to achieve FRET in even larger nanocrystals with different morphologies. Accordingly, we examined the suitability of $NaGdF_4$:Yb/Tm nanorods, having an average diameter of 35 nm and a length of 138 nm, as energy donors of excitation energy. Despite the unfavorable large size of crystals, we obtained an approximately 55% efficiency as a result of Gd-mediated energy migration (Figure S14).

The much improved energy-donating efficiency enabled by migration coupling offers great opportunities for the promotion of many chemical processes such as remote-controlled drug delivery.[12] As a proof of concept, we conjugated silica-coated $NaGdF_4$:Yb/Tm@$NaGdF_4$ nanoparticles with a caged compound bearing a photocleavable 1-naphthol moiety, as shown in Figure 7 and Figure S15.[13] Uncaging after 980 nm excitation was monitored by measuring the steady-state fluorescence emission of 1-naphthol (Figures S16 and S17). To our delight, the caged substrates were released from the nanoparticles in a high yield (~80%) upon photoactivation for 40 min. By comparison, $NaYF_4$-based particle controls yielded only ~10% of the substrates (Figure 7). Note that when coupled to $NaGdF_4$-based core−shell nanoparticles the photocaged 1-naphthol shows a release rate constant of $\sim 2.1 \times 10^{-2}$ min^{-1}, which is almost an order of magnitude faster than that of $NaYF_4$-based controls ($k = 2.3 \times 10^{-3}$ min^{-1}). Clearly, the rate of 1-naphthol release is promoted by the unique ability of Gd^{3+} to migrate the excitation energy, extracted from the high-lying $^1I_6$ state of Tm^{3+} to the shell layer of the nanoparticles (Figure S18).

DOI: 10.1021/jacs.6b09349
J. Am. Chem. Soc. 2016, 138, 15972−15979

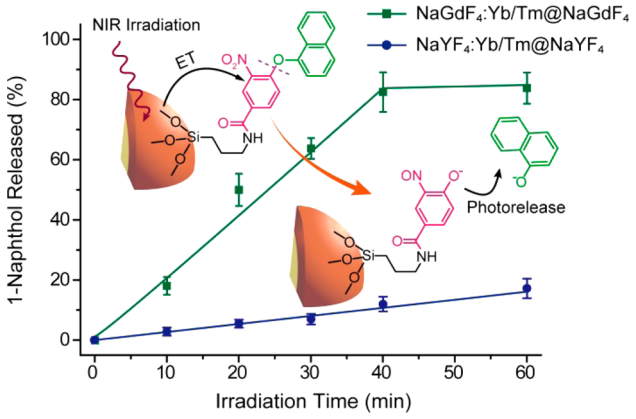

Figure 7. Amount of caged compound (1-naphthol) released was plotted as a function of illumination time for two different sets of upconversion nanoparticles ($NaGdF_4$:Yb/Tm@$NaGdF_4$ and $NaYF_4$:Yb/Tm@$NaYF_4$). All experiments were conducted under 980 nm illumination at a power density of 15 W cm^{-2}. To minimize the laser-induced heating effect, the samples were kept in an ice bath, and the laser beam was blocked off for 1 min after every 5 min of irradiation. Inset: Schematic of the 1-naphthol release from its photocaged form triggered by migration-coupled FRET. The error bars correspond to standard deviation and are based on the statistics of four parallel measurements.

CONCLUSIONS

In conclusion, we have demonstrated that the limited efficiency of the FRET process, imposed by the critical transfer distance, can be overcome by leveraging long-range energy migration through Gd sublattices. This effect has been harnessed in the realization of resonance energy transfer involving large-sized particle donors. The strategies implemented here, including the use of migration coupling process to confine the excitation energy at the particle surface, can principally be extended to other classes of nanoparticles and offer a unique solution for energy transport at large distances. As the long lifetime of lanthanide-based donor emission under study leads to a rather long decay time (~500 μs) in dye acceptor emission, another interesting prospect of the work would be to investigate widely unexplored properties of the dye acceptors with long-lived luminescence.

EXPERIMENTAL SECTION

Reagents. $Gd(CH_3CO_2)_3{\cdot}xH_2O$ (99.9%), $Y(CH_3CO_2)_3{\cdot}xH_2O$ (99.9%), $Yb(CH_3CO_2)_3{\cdot}4H_2O$ (99.9%), $Tm(CH_3CO_2)_3{\cdot}xH_2O$ (99.9%), NaOH (98+%), NH_4F (98+%), 1-octadecene (90%), oleic acid (90%), tetraethylorthosilicate (TEOS, >99.0%), (3-aminopropyl)-triethoxysilane (APTES, >98%), FITC, polyvinylpyrrolidone (PVP K30, average molecular weight = 40 000), 4-bromomethyl-3-nitrobenzoic acid (97%), 1-naphthol (99+%), *N*-hydroxysuccinimide (NHS, 98%), and *N*,*N*′-dicyclohexylcarbodiimide (DCC, 99%) were purchased from Sigma-Aldrich. Anhydrous solvents for organic synthesis were stored over activated molecular sieves (4 Å). Unless otherwise noted, all chemicals were used as received without further purification.

Synthesis of Photocaged 1-Naphthol. *3-Nitro-4-(bromomethyl)-N-(3-(triethoxysilyl)propyl)benzamide.* NHS (575 mg; 5 mmol) and 4-bromomethyl-3-nitrobenzoic acid (1040 mg; 4 mmol) were dissolved with an anhydrous THF solution (10 mL) in a 50 mL three-neck round-bottom flask (Supplementary Scheme 1). To this mixture was slowly added, at 0 °C under an argon atmosphere, another 10 mL of anhydrous THF containing DCC (1032 mg; 5 mmol). The resulting mixture was then stirred in an ice bath for 2 h, followed by filtration to remove solid precipitates. The filtrate was collected and added with APTES (897 mg; 4.05 mmol) and stirred overnight at room temperature. The reaction mixture was concentrated under reduced pressure. The residue was purified by column chromatography on silica gel with a mixed eluent (hexane/ethyl acetate; 5/2) to give the product (1102 mg; yield: 59.5%) as a pale yellow liquid: ^{1}H NMR (300 MHz, $CDCl_3$, 25 °C, TMS) δ = 8.464 (d, J = 1.8 Hz, 1H), 8.095 (dd, J_1 = 8.1 Hz, J_2 = 1.8 Hz, 1H), 7.684 (d, J = 8.1 Hz, 1H), 7.000 (br, 1H), 4.875 (s, 2H), 3.870 (q, J = 6.9 Hz, 6H), 3.527 (q, J = 6.3 Hz, 2H), 1.822 (m, 2H), 1.250 (t, J = 6.9 Hz, 9H), 0.757 (t, J = 7.8 Hz, 2H); ^{13}C NMR (100 MHz, $CDCl_3$, 25 °C) δ = 164.5, 147.7, 136.4, 135.4, 132.9, 132.2, 123.2, 58.5, 42.5, 28.2, 22.7, 18.3, 7.87.

Triethoxysilane-Linked Photocaged 1-Naphthol. To a 50 mL three-neck round-bottom flask charged with 20 mL of anhydrous acetone were added 1-naphthol (350 mg; 2.43 mmol) and potassium carbonate (1000 mg; 7.24 mmol). Subsequently, an anhydrous THF solution (10 mL) of the as-synthesized benzamide compound (1102 mg; 2.38 mmol) was slowly added to the mixture. The reaction mixture was refluxed for 3 h under an argon atmosphere. After being cooled, the product was concentrated and purified by column chromatography on silica gel with a mixed eluent of hexane and ethyl acetate (5:1) to afford the product (1024 mg; yield: 81.8%) as a yellow solid: ^{1}H NMR (300 MHz, $CDCl_3$, 25 °C, TMS) δ = 8.605 (d, J = 1.5 Hz, 1H), 8.295–8.404 (m, 1H), 8.165 (ddd, J_1 = 8.1 Hz, J_2 = 1.5 Hz, J_3 = 8.1 Hz, 2H), 7.779–7.882 (m, 1H), 7.439–7.585 (m, 3H), 7.376 (t, J = 8.1 Hz, 1H), 6.932 (br, 1H), 6.856 (d, J = 7.8 Hz, 1H), 5.700 (s, 2H), 3.877 (q, J = 6.9 Hz, 6H), 3.545 (q, J = 6.3 Hz, 2H), 1.851 (m, 2H), 1.245 (t, J = 6.9 Hz, 9H), 0.761 (t, J = 7.8 Hz, 2H); ^{13}C NMR (100 MHz, $CDCl_3$, 25 °C) δ = 164.7, 153.5, 146.8, 136.9, 135.4, 134.7, 132.5, 128.9, 127.7, 126.7, 125.6, 123.5, 121.7, 121.3, 105.6, 66.8, 58.6, 42.3, 22.7, 18.3, 7.91; MS (ESI) m/z 549.07, calcd for $[M + Na]^+$ 549.20.

Synthesis of Upconversion Nanoparticles. The nanoparticles were synthesized according to a previously reported method.[14] Notably, the method has proven to be effective for preparing $NaGdF_4$- or $NaYF_4$-based core or core–shell nanoparticles with hexagonal phase and narrow size distribution. To achieve similar luminescence performance for two different types of upconversion nanoparticles, the doping concentration of Yb^{3+} and Tm^{3+} was adjusted to 49/1 and 30/0.5 mol % in $NaGdF_4$ and $NaYF_4$ nanoparticles, respectively. Further details are in the Supporting Information.

Preparation of Ligand-Free Upconversion Nanoparticles. The as-prepared oleic-acid-capped upconversion nanoparticles were dispersed in a solution of water/ethanol (v/v = 1:1) containing HCl (0.1 M) and ultrasonicated for 15 min to remove the surface ligands. After the reaction, the nanoparticles were collected by centrifugation at 16 500 rpm for 20 min and further purified using an acidic ethanol solution (pH <4; prepared by addition of 0.1 M HCl to absolute ethanol). The resulting products were washed with ethanol/deionized water several times and redispersed in deionized water.

Preparation of FITC-Conjugated Upconversion Nanoparticles. In a typical experiment, a water dispersion of ligand-free upconversion nanoparticles (500 μL, 0.1 M in lanthanide concentration for core–shell nanoparticles or 0.05 M for core nanoparticles only) was first added to an ethanol solution (5 mL) of PVP (100 mg). The resulting mixture was ultrasonicated for 30 min followed by stirring at room temperature for 24 h. Thereafter, $NH_3{\cdot}H_2O$ (200 μL, 25 wt %), TEOS (5 μL), and APTES (1 μL) were added. After being stirred at room temperature for 12 h, FITC (0–10 μM) was added, and the mixture was stirred at room temperature for another 12 h. The resulting nanoparticles were collected via centrifugation at 16 500 rpm for 30 min, washed with ethanol and deionized water three times, and redispersed in deionized water. The loading concentration of FITC was then determined fluorometrically using a calibration curve involving a set of six standard points (Figure S8 and Table S1).

Preparation of 1-Naphthol-Conjugated Upconversion Nanoparticles. In a typical procedure, a water dispersion of ligand-free upconversion nanoparticles (500 μL, 0.1 M in lanthanide concentration for core–shell nanoparticles or 0.05 M for core nanoparticles only) was first added to an ethanol solution (5 mL) of

DOI: 10.1021/jacs.6b09349
J. Am. Chem. Soc. 2016, 138, 15972–15979

PVP (100 mg). The mixture was ultrasonicated for 30 min and then stirred at room temperature for 24 h. Thereafter, $NH_3 \cdot H_2O$ (200 μL, 25 wt %) and TEOS (5 μL) were added and stirred at room temperature for 2 h, at which time triethoxysilane-modified 1-naphthol (0.2 mg) was added to the mixture. Upon reaction at room temperature for 24 h, the nanoparticles were collected by centrifugation, washed with ethanol and deionized water three times, and redispersed in deionized water.

Characterization. ^{1}H NMR spectra were recorded on a Bruker Avance 300 MHz spectrometer. Chemical shifts (δ, ppm) were reported using TMS as an internal reference. ^{13}C NMR spectra were measured on a Bruker Avance III 400 MHz spectrometer. Mass spectra were performed on a Finnigan LCQ mass spectrometer with electrospray ionization (ESI). TEM measurements were carried out on a JEOL-2010F transmission electron microscope operating at an acceleration voltage of 200 kV. Fourier transform infrared spectroscopy spectra were obtained on a Varian 3100 FT-IR spectrometer. UV−vis transmission spectra were recorded on a SHIMADZU UV-2450 spectrophotometer. Fluorescence spectroscopic studies were carried out on a Jobin-Yvon Fluoromax-4 spectrofluorometer. Upconversion luminescence spectra were obtained with a DONGWOO DM150i monochromator equipped with a R928 photon counting photomultiplier tube, in conjunction with a 980 nm continuous wave diode laser. The luminescence decay curves were measured with a phosphorescence lifetime spectrometer (FSP920, Edinburgh) equipped with a tunable nanosecond OPO laser as the excitation source (680−2300 nm, NT352A, Ekspla). The effective lifetimes were determined by

$$\tau_{\text{eff}} = \frac{1}{I_0}\int_0^\infty I(t)\mathrm{d}t$$

where I_0 and $I(t)$ represent the maximum luminescence intensity and luminescence intensity at time t after cutoff of the excitation light, respectively. Digital photographs were taken with a Nikon D700 camera.

■ ASSOCIATED CONTENT

Supporting Information

The Supporting Information is available free of charge on the ACS Publications website at DOI: 10.1021/jacs.6b09349.

Additional experimental details (PDF)

■ AUTHOR INFORMATION

Corresponding Authors

*iamwhuang@njtech.edu.cn

*chmlx@nus.edu.sg

ORCID

Runfeng Chen: 0000-0003-0222-0296

Wei Huang: 0000-0001-7004-6408

Author Contributions

‖R.D. and J.W. contributed equally to this work.

Notes

The authors declare no competing financial interest.

■ ACKNOWLEDGMENTS

This work is supported by the Singapore Ministry of Education (Grants R143000627112 and R143000642112), National Research Foundation, Prime Minister's Office, Singapore under its Competitive Research Program (CRP Award No. NRF-CRP15-2015-03), National Basic Research Program of China (973 Program, Grant 2015CB932200), National Natural Science Foundation of China (61136003), and the CAS/SAFEA International Partnership Program for Creative Research Teams.

■ REFERENCES

(1) (a) Förster, T. *Ann. Phys.* **1948**, *437*, 55. (b) Jares-Erijman, E. A.; Jovin, T. M. *Nat. Biotechnol.* **2003**, *21*, 1387. (c) Roy, R.; Hohng, S.; Ha, T. *Nat. Methods* **2008**, *5*, 507. (d) Medintz, I. L.; Clapp, A. R.; Mattoussi, H.; Goldman, E. R.; Fisher, B.; Mauro, J. M. *Nat. Mater.* **2003**, *2*, 630. (e) Eliseeva, S. V.; Bünzli, J. C. G. *Chem. Soc. Rev.* **2010**, *39*, 189. (f) Hardin, B. E.; Hoke, E. T.; Armstrong, P. B.; Yum, J. H.; Comte, P.; Torres, T.; Fréchet, J. M. J.; Nazeeruddin, M. K.; Grätzel, M.; McGehee, M. D. *Nat. Photonics* **2009**, *3*, 406.

(2) (a) Clapp, A. R.; Medintz, I. L.; Uyeda, H. T.; Fisher, B. R.; Goldman, E. R.; Bawendi, M. G.; Mattoussi, H. *J. Am. Chem. Soc.* **2005**, *127*, 18212. (b) Liu, N.; Tang, M. L.; Hentschel, M.; Giessen, H.; Alivisatos, A. P. *Nat. Mater.* **2011**, *10*, 631. (c) Mongin, C.; Garakyaraghi, S.; Razgoniaeva, N.; Zamkov, M.; Castellano, F. N. *Science* **2016**, *351*, 369. (d) Koole, R.; Liljeroth, P.; de Mello Donegá, C.; Vanmaekelbergh, D.; Meijerink, A. *J. Am. Chem. Soc.* **2006**, *128*, 10436. (e) Li, J.; Cushing, S. K.; Meng, F.; Senty, T. R.; Bristow, A. D.; Wu, N. *Nat. Photonics* **2015**, *9*, 601. (f) Jung, J. H.; Cheon, D. S.; Liu, F.; Lee, K. B.; Seo, T. S. *Angew. Chem., Int. Ed.* **2010**, *49*, 5708. (g) Wang, L.; Yan, R.; Huo, Z.; Wang, L.; Zeng, J.; Bao, J.; Wang, X.; Peng, Q.; Li, Y. *Angew. Chem., Int. Ed.* **2005**, *44*, 6054. (h) Zhou, B.; Shi, B.; Jin, D.; Liu, X. *Nat. Nanotechnol.* **2015**, *10*, 924. (i) Li, X.; Zhang, F.; Zhao, D. *Chem. Soc. Rev.* **2015**, *44*, 1346. (j) Yang, D.; Ma, P.; Hou, Z.; Cheng, Z.; Li, C.; Lin, J. *Chem. Soc. Rev.* **2015**, *44*, 1416. (k) Li, Z.; Lv, S.; Wang, Y.; Chen, S.; Liu, Z. *J. Am. Chem. Soc.* **2015**, *137*, 3421. (l) Liu, J.; Liu, Y.; Bu, W.; Bu, J.; Sun, Y.; Du, J.; Shi, J. *J. Am. Chem. Soc.* **2014**, *136*, 9701. (m) Zhou, Y.; Pei, W.; Zhang, X.; Chen, W.; Wu, J.; Yao, C.; Huang, L.; Zhang, H.; Huang, W.; Loo, J. S. C.; Zhang, Q. *Biomaterials* **2015**, *54*, 34. (n) Wu, X.; Zhang, Y.; Takle, K.; Bilsel, O.; Li, Z.; Lee, H.; Zhang, Z.; Li, D.; Fan, W.; Duan, C.; Chan, E. M.; Lois, C.; Xiang, Y.; Han, G. *ACS Nano* **2016**, *10*, 1060. (o) Wang, Y.; Liu, K.; Liu, X.; Dohnalova, K.; Gregorkiewicz, T.; Kong, X.; Aalders, M. C. G.; Buma, W. J.; Zhang, H. *J. Phys. Chem. Lett.* **2011**, *2*, 2083. (p) Wu, M.; Wang, X.; Wang, K.; Guo, Z. *Chem. Commun.* **2016**, *52*, 8377.

(3) Clapp, A. R.; Medintz, I. L.; Mauro, J. M.; Fisher, B. R.; Bawendi, M. G.; Mattoussi, H. *J. Am. Chem. Soc.* **2004**, *126*, 301.

(4) Almgren, M.; Löfroth, J. E. *J. Chem. Phys.* **1982**, *76*, 2734.

(5) (a) Berberan-Santos, M. *Am. J. Phys.* **1986**, *54*, 1139. (b) Berberan-Santos, M.; Prieto, M. J. E. *J. Chem. Soc., Faraday Trans. 2* **1987**, *83*, 1391. (c) Rabouw, F. T.; den Hartog, S. A.; Senden, T.; Meijerink, A. *Nat. Commun.* **2014**, *5*, 3610.

(6) De Vries, A. J.; Minks, B. P.; Blasse, G. *J. Lumin.* **1988**, *39*, 153.

(7) (a) Soos, Z. G.; Powell, R. C. *Phys. Rev. B* **1972**, *6*, 4035. (b) Burshteĭn, A. I. *Sov. Phys. Usp.* **1984**, *27*, 579. (c) Powell, R. C.; Blasse, G. *Struct. Bonding (Berlin, Ger.)* **1980**, *42*, 43.

(8) (a) Debasu, M. L.; Ananias, D.; Rocha, J.; Malta, O. L.; Carlos, L. D. *Phys. Chem. Chem. Phys.* **2013**, *15*, 15565. (b) Wang, F.; Deng, R.; Wang, J.; Wang, Q.; Han, Y.; Zhu, H.; Chen, X.; Liu, X. *Nat. Mater.* **2011**, *10*, 968. (c) Su, Q.; Han, S.; Xie, X.; Zhu, H.; Chen, H.; Chen, C. K.; Liu, R.; Chen, X.; Wang, F.; Liu, X. *J. Am. Chem. Soc.* **2012**, *134*, 20849. (d) Tu, L.; Liu, X.; Zhang, H. *Chem. Soc. Rev.* **2015**, *44*, 1331. (e) Zhou, B.; Yang, W.; Han, S.; Sun, Q.; Liu, X. *Adv. Mater.* **2015**, *27*, 6208.

(9) (a) Wegh, R. T.; Donker, H.; Oskam, K. D.; Meijerink, A. *Science* **1999**, *283*, 663. (b) Cao, C.; Qin, W.; Zhang, J.; Wang, Y.; Zhu, P.; Wei, G.; Wang, G.; Kim, R.; Wang, L. *Opt. Lett.* **2008**, *33*, 857.

(10) (a) Haase, M.; Schafer, H. *Angew. Chem., Int. Ed.* **2011**, *50*, 5808. (b) Auzel, F. *Chem. Rev.* **2004**, *104*, 139. (c) Kebaïli, I.; Dammak, M.; Cavalli, E.; Bettinelli, M. *J. Lumin.* **2011**, *131*, 2010. (d) Mi, Z.; Zhang, Y.; Vanga, S. K.; Chen, C. B.; Tan, H.; Watt, F.; Liu, X.; Bettiol, A. A. *Nat. Commun.* **2015**, *6*, 8832. (e) Deng, R.; Qin, F.; Chen, R.; Huang, W.; Hong, M.; Liu, X. *Nat. Nanotechnol.* **2015**, *10*, 237. (f) Zhong, Y.; Tian, G.; Gu, Z.; Yang, Y.; Gu, L.; Zhao, Y.; Ma, Y.; Yao, J. *Adv. Mater.* **2014**, *26*, 2831. (g) Han, S.; Qin, X.; An, Z.; Zhu, Y.; Liang, L.; Han, Y.; Huang, W.; Liu, X. *Nat. Commun.* **2016**, *7*, 13059.

(11) Bednarkiewicz, A.; Nyk, M.; Samoc, M.; Strek, W. *J. Phys. Chem. C* **2010**, *114*, 17535.

DOI: 10.1021/jacs.6b09349
J. Am. Chem. Soc. 2016, 138, 15972−15979

(12) (a) Dong, H.; Du, S.; Zheng, X.; Lyu, G.; Sun, L.; Li, L.; Zhang, P.; Zhang, C.; Yan, C. *Chem. Rev.* **2015**, *115*, 10725. (b) LaVan, D. A.; McGuire, T.; Langer, R. *Nat. Biotechnol.* **2003**, *21*, 1184. (c) Li, W.; Wang, J.; Ren, J.; Qu, X. *J. Am. Chem. Soc.* **2014**, *136*, 2248. (d) Carling, C. J.; Nourmohammadian, F.; Boyer, J. C.; Branda, N. R. *Angew. Chem., Int. Ed.* **2010**, *49*, 3782. (e) Wu, S.; Butt, H. J. *Adv. Mater.* **2016**, *28*, 1208. (f) Yang, Y.; Shao, Q.; Deng, R.; Wang, C.; Teng, X.; Cheng, K.; Cheng, Z.; Huang, L.; Liu, Z.; Liu, X.; Xing, B. *Angew. Chem., Int. Ed.* **2012**, *51*, 3125. (g) Lai, J.; Zhang, Y.; Pasquale, N.; Lee, K. B. *Angew. Chem., Int. Ed.* **2014**, *53*, 14419.

(13) Holmes, C. P. *J. Org. Chem.* **1997**, *62*, 2370.

(14) (a) Wang, F.; Wang, J.; Liu, X. *Angew. Chem., Int. Ed.* **2010**, *49*, 7456. (b) Wang, F.; Deng, R.; Liu, X. *Nat. Protoc.* **2014**, *9*, 1634.

DOI: 10.1021/jacs.6b09349
J. Am. Chem. Soc. 2016, 138, 15972−15979